

Renormalization factors of quark bilinears using the D_{CI} operator with dynamical quarks

Philipp Huber

Institut f. Physik, FB Theoretische Physik, Universität Graz

E-mail: philipp.huber@uni-graz.at

ABSTRACT: Non-perturbative renormalization factors of bilinear quark operators are computed for the Chirally Improved lattice action with two dynamic quarks. The analysis is based on five different parameter sets with lattice size $12^3 \times 24$ and four parameter sets with lattice size $16^3 \times 32$. For the pseudoscalar renormalization factor the pion pole contribution is subtracted and chiral extrapolations are performed. Results are given in RI'- and $\overline{\text{MS}}$ -scheme as well as in RGI-form.

KEYWORDS: Lattice field theory, renormalization, chiral lattice fermions, Chirally Improved Dirac operator, dynamic quarks.

Contents

1. Motivation	1
2. Method	2
3. Technicalities	5
3.1 Parameters	5
3.2 Interpolation, pole contributions and chiral limit	5
4. Results	8
4.1 Results in the RI'-scheme	8
4.2 Results in the $\overline{\text{MS}}$ -scheme	9
4.3 Results in the RGI-form	13
4.4 Collection of Results	15
5. Summary and Conclusion	17

1. Motivation

In order to determine renormalized quantities like quark masses, the chiral condensate or the pion decay constant on the lattice one needs renormalization factors to compare with results from experiments or continuum theories. Those values are typically given in the modified minimal subtraction ($\overline{\text{MS}}$) renormalization scheme.

Lattice Dirac operators satisfying the Ginsparg-Wilson (GW) equation [1] implement a version of chiral symmetry that is closest to the continuum form, with only local $\mathcal{O}(a)$ violations. Exact GW-operators have the benefit of relations that simplify the renormalization procedure [2]. For Dirac operators that fulfill the GW-equation only approximately computing renormalization factors also provides a check how well chiral symmetry is realized in this formulation.

Let us consider local, flavor non-singlet bilinear quark-field operators

$$O_\Gamma = \bar{u} \Gamma d, \tag{1.1}$$

where Γ denotes a matrix from the Clifford algebra in the chiral representation and u and d denote the quark fields for the light quarks. We organize the 16 matrices into the scalar, vector, tensor, axial vector and pseudoscalar sectors with $S \sim \mathbb{1}, V \sim \gamma_\mu, T \sim \frac{i}{2} [\gamma_\mu, \gamma_\nu], A \sim \gamma_\mu \gamma_5, P \sim \gamma_5$ according to their properties under Lorentz transformations. For a chiral Dirac operator we have $Z_P = Z_S$ and $Z_A = Z_V$. For conserved covariant currents we have $Z_A = 1$ due to Ward identities.

Although only the overlap operator [3, 4] satisfies the GW-equation exactly, there is a number of formulations that have good chiral properties by satisfying the GW-constraint approximately (fixed point operator [5], D_{CI} [6]) or in some limit (domain wall fermions [7, 8]). Within the BGR-collaboration fixed point and CI operators have been studied in both, the quenched approximation [9] and the CI operator was analyzed in full QCD in [10, 11, 12].

The D_{CI} has been introduced in [6, 13] as an approximate solution to the GW-equation, where the lattice derivative operator does not only include nearest neighbor interactions, but also more remote connection, each of which carries a Dirac structure.

Renormalization factors for the quenched case have been computed in [14] and this work follows the procedure therein closely. Non-perturbative renormalization in the quenched approximation has also been performed for the Wilson operator [15, 16, 17, 18], staggered fermions [19], domain-wall fermions [20] and the overlap operator [21, 22, 23]. Calculations with dynamic fermions were performed non-perturbatively for the overlap operator in [24]. For dynamical clover fermions perturbative results were presented in [25, 26], while [27] covers perturbative and non-perturbative approaches.

In Sect. 2 the method to determine renormalization constants [28] is reviewed. Technicalities like the parameters used for generating gauge configurations and data analysis are dealt with in Sect. 3. Results in different schemes are discussed in Sect. 4.1, Sect. 4.2 and Sect. 4.3 and we summarize our results and conclude in Sect. 5.

2. Method

We want to compute non-perturbative renormalization constants on the lattice using a scheme applicable in both, lattice simulations and perturbative continuum calculations. To this end we use the regularization independent scheme (RI) proposed in [28]. Results in the RI-scheme can also be converted to the more conventional $\overline{\text{MS}}$ -scheme in a perturbative way. In the RI-scheme we match expectation values of bilinear quark operators between quark fields at a specific momentum value $p^2 = \mu^2$ with the renormalization scale μ ,

$$\langle p | O_{\Gamma} | p \rangle|_{p^2=\mu^2} \quad (2.1)$$

to corresponding tree-level matrix elements $\langle p | O_{\Gamma} | p \rangle_0$. Continuum perturbation theory can only be applied for a renormalization scale much larger than the QCD scale parameter Λ_{QCD} . Discretization effects can be neglected for μ much smaller than the lattice cut-off $1/a$ so the renormalization procedure is expected to work in a window

$$\Lambda_{\text{QCD}}^2 \ll \mu^2 \ll 1/a^2. \quad (2.2)$$

Expression (2.1) is gauge-variant so we need to fix the gauge in order to compare results obtained in a lattice formulation to continuum results. Landau gauge can be implemented in both approaches, but has the problem of Gribov ambiguities. In [29, 30, 31, 14] this has been addressed and no significant effects were detected, therefore no explicit check was performed in this work.

We use the method from [28] with the modifications from [32] to compute renormalization factors. Multiplying (2.1) with the inverse of the tree-level matrix element $\langle p|O_\Gamma|p\rangle_0^{-1}$ gives us the renormalization condition

$$Z_\Gamma \frac{1}{12} \text{Tr} \left[\langle p|O_\Gamma|p\rangle \langle p|O_\Gamma|p\rangle_0^{-1} \right] \Big|_{p^2=\mu^2} = 1. \quad (2.3)$$

The matrix element

$$\langle p|O_\Gamma|p\rangle = \frac{1}{Z_q} \Lambda_\Gamma(p) \quad (2.4)$$

with the quark field renormalization factor Z_q is proportional to the amputated Green function

$$\Lambda_\Gamma(p) = S^{-1}(p) G_\Gamma(p) S^{-1}(p). \quad (2.5)$$

The inverse quark propagator is denoted $S^{-1}(p)$. The Green function $G_\Gamma(p)$ is computed by taking the expectation value of the local operator $O_\Gamma(z)$ and Fourier transforming it. This reads

$$G_\Gamma(p)_{\alpha,\beta} = \frac{1}{V} \sum_{x,y} e^{-ip(x-y)} \left\langle u_\alpha(x) \sum_z O_\Gamma(z) \bar{d}_\beta(y) \right\rangle, \quad (2.6)$$

where the indices α, β run over color and Dirac indices and V denotes the lattice volume. We use equal masses for u and d quarks, hence the quark propagator is

$$S_{\alpha,\beta}(x,y) = \langle u_\alpha(x) \bar{u}_\beta(y) \rangle = \langle d_\alpha(x) \bar{d}_\beta(y) \rangle. \quad (2.7)$$

Using the modification [32] we compute quark propagators with momentum sources

$$S_n(x|p) = \sum_y e^{ipy} S_n(x,y) \quad (2.8)$$

for each gauge configuration. Inserting the local operator defined in Eq. (1.1) into Eq. (2.6) we can rewrite $G_\Gamma(p)$ in terms of the quark propagator $S(x|p)$. Using γ_5 -hermiticity, we rewrite the Green function

$$\begin{aligned} G_\Gamma(p) &= \frac{1}{V} \sum_{x,y,z} e^{-ip(x-y)} \langle u_\alpha(x) \bar{u}_\beta(z) \Gamma d_\alpha(z) \bar{d}_\beta(y) \rangle \\ &\approx \frac{1}{VN} \sum_{n=1}^N \sum_z \gamma_5 S_n(z|p)^\dagger \gamma_5 \Gamma S_n(z|p), \end{aligned} \quad (2.9)$$

where N is the number of gauge configurations we average over. The quark propagator in momentum space is obtained by transforming Eq. (2.8) fully to momentum space

$$S(p) \approx \frac{1}{VN} \sum_{n=1}^N \sum_x e^{-ipx} S_n(x|p). \quad (2.10)$$

We use momentum sources [32] with momenta listed in Table 2 and Table 3 in order to compute $S_n(y|p)$ by solving

$$\sum_y D_{\text{CI}}(x,y) S_n(y|p) = e^{ipx} \quad (2.11)$$

for the chirally improved Dirac operator D_{CI} . This implies we have to solve Eq. (2.11) for every momentum vector, but improves the signal significantly. In momentum space this Dirac operator reading

$$D_{\text{CI}}(p) = R(p) + i\gamma_\mu a_\mu(p) \quad (2.12)$$

in the free massless case is constructed using the functions [6, 13]

$$a_\mu(p) = ip_\mu + \mathcal{O}(ap)^2 \quad \text{and} \quad R(p) = \mathcal{O}(ap)^2. \quad (2.13)$$

The quark field renormalization is obtained in the so-called RI'-scheme, where we can apply Eq. (2.12) and find

$$\begin{aligned} Z_q^{\text{RI}'}(p) &= \frac{1}{12} \text{Tr} S^{-1}(p) S_0(p) \Big|_{p^2=\mu^2} \\ &= \frac{1}{12} \text{Tr} \left(S^{-1}(p) \frac{R(p) - i a_\mu(p) \gamma_\mu}{R(p)^2 + a_\mu(p) a_\mu(p)} \right) \Big|_{p^2=\mu^2}. \end{aligned} \quad (2.14)$$

Renormalization factors for quark bilinears can then be computed from the renormalization condition Eq. (2.3) together with the definitions Eq. (2.4) and Eq. (2.5) for the RI'-scheme

$$\begin{aligned} Z_\Gamma^{\text{RI}'}(p) &= \frac{12}{\text{Tr} \left[\langle p | O_\Gamma | p \rangle \langle p | O_\Gamma | p \rangle_0^{-1} \right]} \Big|_{p^2=\mu^2} \\ &= \frac{12 Z_q^{\text{RI}'}(p)}{\text{Tr} [S^{-1}(p) G_\Gamma(p) S^{-1}(p) \Gamma^{-1}]} \Big|_{p^2=\mu^2}, \end{aligned} \quad (2.15)$$

where we use $\langle p | O_\Gamma | p \rangle_0 = \Gamma$. For the vector, axial vector and tensor sectors we average over the components before taking the trace.

A modified version of the method described above was presented in [33] and also in [34], which will be referred to as the “reduced” method. The contribution that comes with the unit matrix of the quark propagator introduces a pure cut-off effect and should therefore be eliminated from the renormalization prescription. A way to achieve this is to define a reduced quark propagator

$$\overline{S}(p) = S(p) - \left(\frac{1}{12} \text{Tr} S(p) \right) \mathbb{1}, \quad (2.16)$$

as well as a reduced free quark propagator

$$\overline{S}_0(p) = S_0(p) - \left(\frac{1}{12} \text{Tr} S_0(p) \right) \mathbb{1}. \quad (2.17)$$

Consequently a reduced quark field renormalization factor

$$\overline{Z}_q^{\text{RI}'}(p) = \frac{1}{12} \text{Tr} \overline{S}^{-1}(p) \overline{S}_0(p) \Big|_{p^2=\mu^2} \quad (2.18)$$

can be computed. Analogously Eq. (2.15) can be redefined in these terms

$$\overline{Z}_\Gamma^{\text{RI}}(p) = \frac{12\overline{Z}_q^{\text{RI}}(p)}{\text{Tr} \left[\overline{S}^{-1}(p) \hat{G}_\Gamma(p) \overline{S}^{-1}(p) \Gamma^{-1} \right]} \Big|_{p^2=\mu^2}, \quad (2.19)$$

with

$$\hat{G}_\Gamma(p) \approx \frac{1}{VN} \sum_{n=1}^N \sum_z \gamma_5 \overline{S}_n(z|p)^\dagger \gamma_5 \Gamma \overline{S}_n(z|p). \quad (2.20)$$

We state the final numbers for the renormalization factors in both, the non-reduced and the reduced scheme.

3. Technicalities

3.1 Parameters

Gauge configurations were generated with two dynamic quarks using the Lüscher-Weisz gauge action [35] and stout smearing [36], which are presented in [10, 11, 12]. Prior results in the quenched approximation utilized hypercubic smearing instead of stout smearing, hence a comparison of renormalization factors for the quenched and the dynamic case are not applicable. The gauge couplings and sea-quark masses are listed in Table 1. For the $12^3 \times 24$ setups we compute 10, for the $16^3 \times 32$ setups 5 momentum propagators for each momentum vector.

run	$L^3 \times T$	β	$a m_q$	$a m_{\text{AWI}}$	$m_{\text{AWI}}[\text{MeV}]$	$a[\text{fm}]$	$a[\text{GeV}^{-1}]$	# cf.
a	$12^3 \times 24$	4.7	-0.05	0.023(2)	30.9(8)	0.147(18)	0.75(9)	10
b	$12^3 \times 24$	5.2	0.02	0.025(1)	42.1(2)	0.115(6)	0.58(3)	10
c	$12^3 \times 24$	5.2	0.03	0.037(1)	58.1(2)	0.125(6)	0.63(3)	10
d	$12^3 \times 24$	5.3	0.04	0.037(2)	60.8(2)	0.120(4)	0.61(2)	10
e	$12^3 \times 24$	5.3	0.05	0.050(19)	76.4(2)	0.129(1)	0.654(5)	10
f	$16^3 \times 32$	4.65	-0.06	0.02664(15)	35.05(19)	0.150(1)	0.760(5)	5
g	$16^3 \times 32$	4.70	-0.05	0.03277(31)	43.11(41)	0.150(2)	0.76(1)	5
h	$16^3 \times 32$	4.58	-0.077	0.01097(26)	15.03(36)	0.144(2)	0.73(1)	5
i	$16^3 \times 32$	4.65	-0.07	0.00861(36)	12.09(52)	0.140(1)	0.711(5)	5

Table 1: Parameters of the different runs with AWI mass and lattice spacing measurements thereon. The lattice spacing and AWI mass values are taken from [12, 10]. For run i the values are preliminary and not yet published. Runs $a - e$ denote runs on the smaller $12^3 \times 24$ lattices, while runs $f - i$ denote the runs on the $16^3 \times 32$ lattices. Note that the lattice spacing a for run a is closer to runs with big lattice size than to the remaining four $12^3 \times 24$ lattices.

3.2 Interpolation, pole contributions and chiral limit

In the quenched case [14] we performed a chiral extrapolation of the renormalization factors using the different valance quark masses for each lattice setup and then stated these values

$a p_1$	$a p_2$	$a p_3$	$a p_4$	$a p$	a $p[\text{GeV}]$	b $p[\text{GeV}]$	c $p[\text{GeV}]$	d $p[\text{GeV}]$	e $p[\text{GeV}]$
0	0	0	0	0.1309	0.1757	0.2246	0.2066	0.2153	0.2002
1	0	0	0	0.3927	0.5271	0.6738	0.6199	0.6458	0.6007
0	0	0	1	0.5397	0.7245	0.9261	0.8520	0.8875	0.8256
1	0	0	1	0.6545	0.8786	1.1230	1.0332	1.0763	1.0012
0	1	1	1	0.9163	1.2300	1.5723	1.4465	1.5068	1.4016
1	1	1	1	0.9883	1.3266	1.6958	1.5601	1.6251	1.5117
2	1	1	1	1.1184	1.5013	1.9191	1.7655	1.8391	1.7108
3	1	1	1	1.2892	1.7306	2.2121	2.0352	2.1200	1.9721
2	1	1	2	1.4399	1.9329	2.4707	2.2730	2.3678	2.2026
3	1	1	2	1.5762	2.1159	2.7047	2.4883	2.5920	2.4111
4	2	2	2	2.1628	2.9033	3.7112	3.4143	3.5565	3.3084

Table 2: The available momentum combinations on the $12^3 \times 24$ lattice. Parameters of the runs are listed in Table 1.

$a p_1$	$a p_2$	$a p_3$	$a p_4$	$a p$	f $p[\text{GeV}]$	g $p[\text{GeV}]$	h $p[\text{GeV}]$	i $p[\text{GeV}]$
2	1	1	1	0.8388	1.1011	1.1035	1.1494	1.1802
3	1	1	1	0.9669	1.2693	1.2720	1.3250	1.3604
2	1	1	2	1.0799			1.4798	
4	1	1	1	1.1151			1.5280	
3	1	1	2	1.1822	1.5519	1.5552	1.6200	1.6633
4	1	1	2	1.3061	1.7146		1.7898	
3	1	2	2	1.3639	1.7904	1.7942	1.8690	1.9189
3	2	2	2	1.5241	2.0007	2.0049	2.0885	2.1443
4	2	2	2	1.6221	2.1294	2.1339	2.2228	2.2822
6	1	2	2	1.7369	2.2801	2.2849	2.3801	2.4437
5	1	2	3	1.8235	2.3938	2.3989	2.4988	
5	2	2	3	1.9462	2.5549	2.5603	2.6670	2.7383

Table 3: The available momentum combinations on the $16^3 \times 32$ lattice. The p values are only listed if we computed the quark propagator for this momentum vector. Parameters of the runs are listed in Table 1.

as our final numbers for Z_Γ . In a full QCD calculation we only have one physical quark mass per lattice setup, so a chiral limit cannot be performed in a straightforward way. In this work we present the renormalization factors for each lattice setup and perform an extrapolation using different valence and sea quark masses, i. e. a partially quenched approximation, only for discussing the continuum limit in Sect. 4.4 and for extracting the pion pole contributions. The pseudoscalar density couples to the Goldstone boson channel, so we expect $\mathcal{O}(1/m)$ contributions to the pseudoscalar propagator in the chiral limit. As

run	$a m_q$	$a m_q$								
a	-0.05	-0.025	0.0	0.03	0.06	0.10				
b	0.02	0.065	0.11	0.155	0.20					
c	0.03	0.0725	0.115	0.1575	0.20					
d	0.04	0.08	0.12	0.16	0.20					
e	0.05	0.875	0.125	0.1625	0.20					
f	-0.06	0.0	0.06							
g	-0.05	0.0	0.05							
h	-0.077	-0.067	-0.057	-0.047	-0.037	-0.027	-0.017	0.003	0.026	0.063
i	-0.07	-0.06	-0.05	-0.04	-0.03	-0.02	-0.01	0.0	0.02	0.04

Table 4: Valence quark masses used in the configurations in Table 1. The second column denotes the case where sea quark mass and valence quark mass are equal, i. e. full dynamic calculations, while the columns three to eleven mark partially quenched situations used for the pion pole extractions in Sect. 3.2.

discussed in [32, 37, 38, 39, 40] the inverse renormalization factor can be expanded as

$$\frac{1}{Z_P} = \frac{A}{m} + B + Cm + \mathcal{O}(m^2) \quad (3.1)$$

and a “subtracted” renormalization factor can be defined by subtracting the pole term

$$\frac{1}{Z_P^{Sub}} = \frac{1}{Z_P} - \frac{A}{m}. \quad (3.2)$$

The operator product expansion ensures that pole contributions are suppressed for large values of μ . For runs $a - e$, h and i we have sufficiently many different valence quark masses and we use the lowest five to perform a fit to Eq. (3.1). For runs f and g we only have three valence quark masses, so here we only solve Eq. (3.1) for the coefficient. The valence quark masses are collected in Table 4. Fig. 1 shows the original and subtracted renormalization factors Z_P and Z_P^{Sub} of runs h and i for selected momentum vectors plotted against the AWI mass including the corresponding fit.

In Fig. 2 the coefficient A of such a fit is displayed for runs $a - e$, h and i . The coefficient A is expected to be proportional to $\langle \bar{q} q \rangle / p^2$, where $-\langle \bar{q} q \rangle = \Sigma$ is the chiral condensate (cf. [24, 41]). In one-loop partially quenched chiral perturbation theory the condensate includes a logarithmic term that leads to a divergence in the chiral limit [42], but a possible additional logarithmic term cannot be disentangled from the $1/m$ pole term with valence quark masses available.¹ Coefficient A shows a rather universal behavior with a estimated uncertainty of 3% for $\langle \bar{q} q \rangle$, which indicates a consistent pion-pole removal over the whole range of lattice configurations. In order to compare runs at the same physical momentum transfer we use a cubic square interpolating fit. The values presented at momentum transfer $\mu = 2 \text{ GeV}$ are taken from such interpolating fits.

Uncertainties of all quantities are calculated using the standard jackknife procedure. Note,

¹Thanks to the referee for pointing this fact out.

however that we include only uncertainties of statistical nature and no systematics due to finite size effects or other artifacts.

For selected momenta we have higher statistics available for run *a* (23 configurations) and *h* (15 configurations) from Table 1. As expected uncertainties are lower for larger ensembles, but in the region with $\mu > 1$ GeV all mean values for the renormalization factors with larger sample number lie within the error band of the results with smaller sample number. Only in the region below 1 GeV we find larger deviations, but those values also come with large uncertainties.

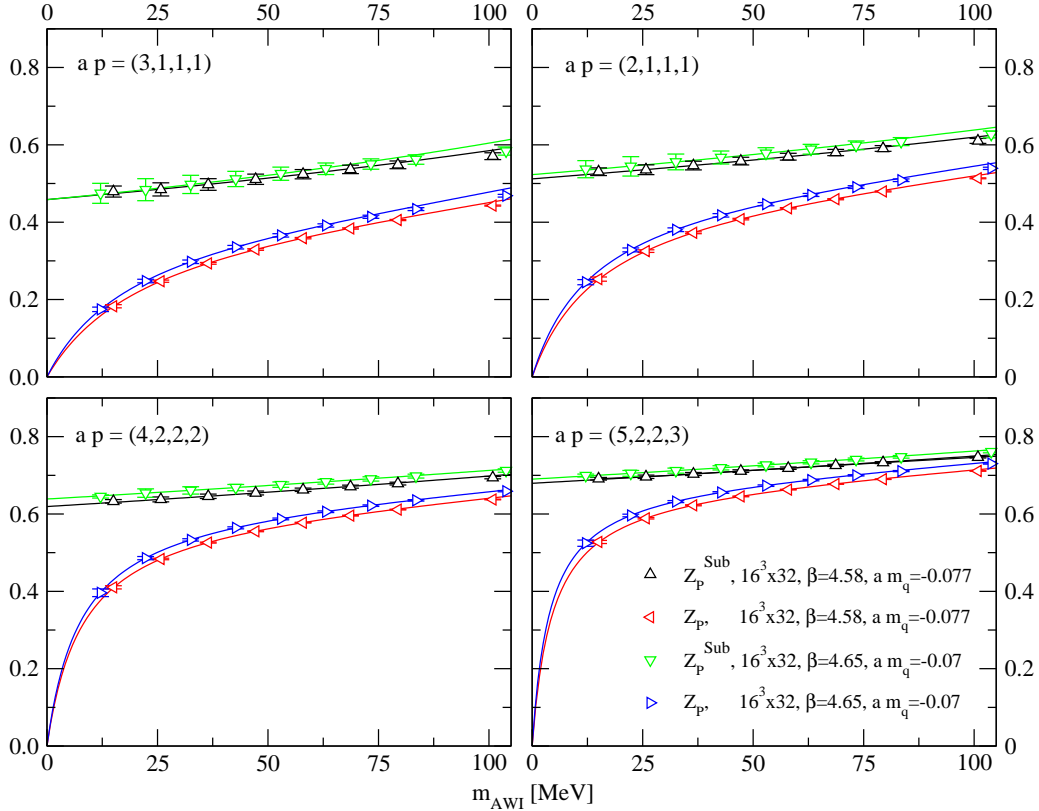


Figure 1: The renormalization factors Z_P and Z_P^{Sub} plotted against the the AWI-mass for selected momenta of runs *h* and *i*. A fit to Eq. (3.1) is shown for Z_P and the same fit with subtracted pole term is plotted for Z_P^{Sub} .

4. Results

4.1 Results in the RI'-scheme

In Fig. 3 and Fig. 4 we present the result of $Z^{RI'}$ plotted against the momentum for runs on $12^3 \times 24$ and $16^3 \times 32$ lattices, respectively. Additionally an interpolating fit is displayed. Runs *b* – *e* seem to agree for most of the quantities, whereas run *a* lies closer to the runs on the $16^3 \times 32$ lattices. Therefore run *a* is also included in the latter plot for comparison. This separation might be a hint for finite size effects, because run *a* has a significantly

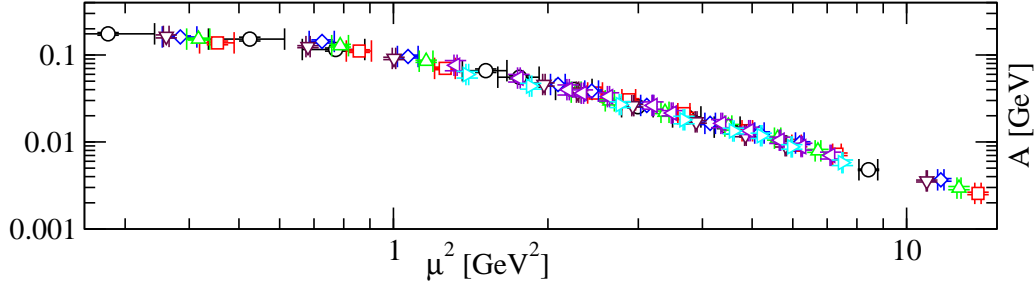


Figure 2: The coefficient A of the fit to Eq. (3.1) displayed against the μ^2 . We plot the runs a (black circles), b (red squares), c (blue diamonds), d (green upwards triangles), e (brown downwards triangles) on the $12^3 \times 24$ lattices and the runs h (violet left pointing triangles) and i (cyan right pointing triangles) on the $16^3 \times 32$ lattices. The parameters of the different runs are presented in Table 1.

larger box size than the rest of the $12^3 \times 24$ setups and also the lattice spacing lies in the region of runs $f - i$.

A chiral operator is expected to have $Z_A = Z_V = \text{const.}$ and $Z_P = Z_S = \text{const.}$. To this end we also plot the ratios $Z_P^{\text{Sub,RI}'} / Z_S^{\text{RI}'} = Z_P^{\text{Sub}} / Z_S$ and $Z_A^{\text{RI}'} / Z_V^{\text{RI}'}$ in Fig. 5, where the scaling behavior is supposed to cancel out. In the interval $1.5 \text{ GeV} < \mu < 3.0 \text{ GeV}$ this is satisfied up to 7% and 10% for $Z_P^{\text{Sub,RI}'} / Z_S^{\text{RI}'}$ and $Z_A^{\text{RI}'} / Z_V^{\text{RI}'}$, respectively, on the larger lattices. The D_{CI} does not satisfying the GW-relation exactly, so we cannot expect the ratios to be equal to unity. In the quenched case [14] a comparable behavior was found for Z_A / Z_V , while Z_P^{Sub} / Z_S was closer to unity. Note, that these ratios are the only quantities that we can directly compare to other studies, as the absolute values of the renormalization factors strongly depend on the formulation of the Dirac operator and the smearing method in use.

4.2 Results in the $\overline{\text{MS}}$ -scheme

The difference between the RI'-scheme we use and the RI-scheme lies solely in the definition of the quark field renormalization factor, hence

$$c_q^{\text{RI}'\text{RI}} = \frac{Z_q^{\text{RI}}}{Z_q^{\text{RI}'}} = \frac{Z_\Gamma^{\text{RI}}}{Z_\Gamma^{\text{RI}'}}. \quad (4.1)$$

The conversion factor expanded in terms of the strong coupling constant α_s in Landau gauge reads [43]

$$c_q^{\text{RI}'\text{RI}} = 1 + \left\{ -\frac{67}{6} + \frac{2N_f}{3} \right\} \left(\frac{\alpha_s}{4\pi} \right)^2 + \left\{ -\frac{52321}{72} + \frac{607\zeta_3}{4} + \left(\frac{2236}{27} - 8\zeta_3 \right) N_f - \frac{52}{27} N_f^2 \right\} \left(\frac{\alpha_s}{4\pi} \right)^3 + \mathcal{O} \left(\frac{\alpha_s}{4\pi} \right)^4, \quad (4.2)$$

where N_f denotes the number of dynamic quarks and ζ_n denotes the Riemann zeta function evaluated at n .

Due to Ward identities the conversion factor for axial vector and vector operators reads

$$c_{V,A}^{\text{RI}'\overline{\text{MS}}} = c_\Gamma^{\text{RI}'\text{RI}} c_{V,A}^{\text{RI}\overline{\text{MS}}} = c_\Gamma^{\text{RI}'\text{RI}} = c_q^{\text{RI}'\text{RI}} \quad \text{i. e.} \quad c_{V,A}^{\text{RI}\overline{\text{MS}}} = 1. \quad (4.3)$$

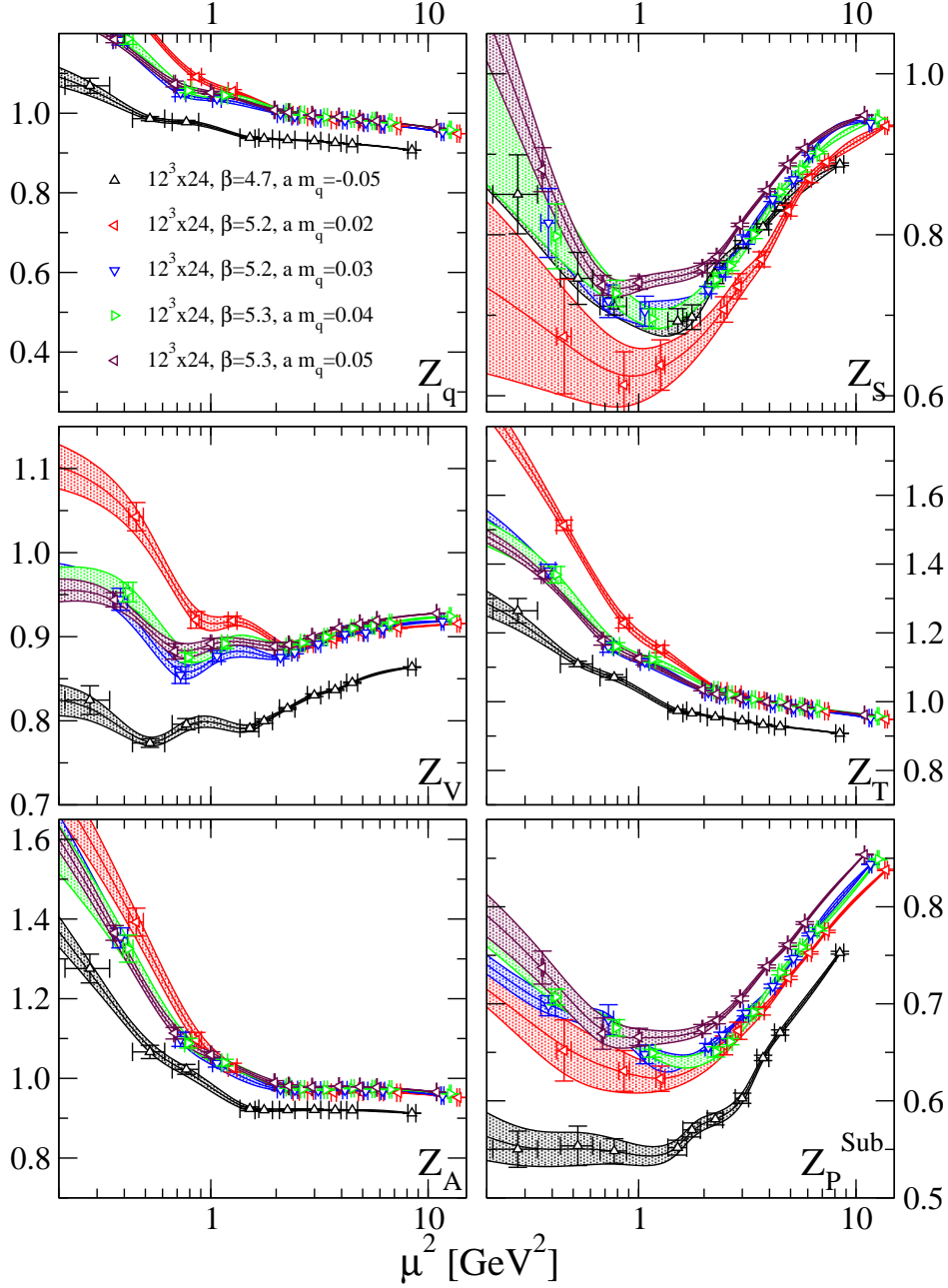


Figure 3: The renormalization factor Z^{RI} displayed against μ^2 for all $12^3 \times 24$ lattices.

For scalar and pseudoscalar sectors we have [44]

$$\begin{aligned}
c_{P,S}^{\text{R}\overline{\text{MS}}} = & 1 + \frac{16}{3} \left(\frac{\alpha_s}{4\pi} \right) + \\
& + \left\{ \frac{2246}{9} - \frac{89N_f}{9} - \frac{152\zeta_3}{3} \right\} \left(\frac{\alpha_s}{4\pi} \right)^2 + \\
& + \left\{ \frac{8290535}{648} - \frac{466375\zeta_3}{108} + \frac{2960\zeta_5}{9} + \right. \\
& + \left(-\frac{262282}{243} + \frac{4936\zeta_3}{27} - \frac{80\zeta_4}{3} \right) N_f + \\
& + \left. \left(\frac{8918}{729} + \frac{32\zeta_3}{27} \right) N_f^2 \right\} \left(\frac{\alpha_s}{4\pi} \right)^3 + \mathcal{O} \left(\frac{\alpha_s}{4\pi} \right)^4.
\end{aligned} \tag{4.4}$$

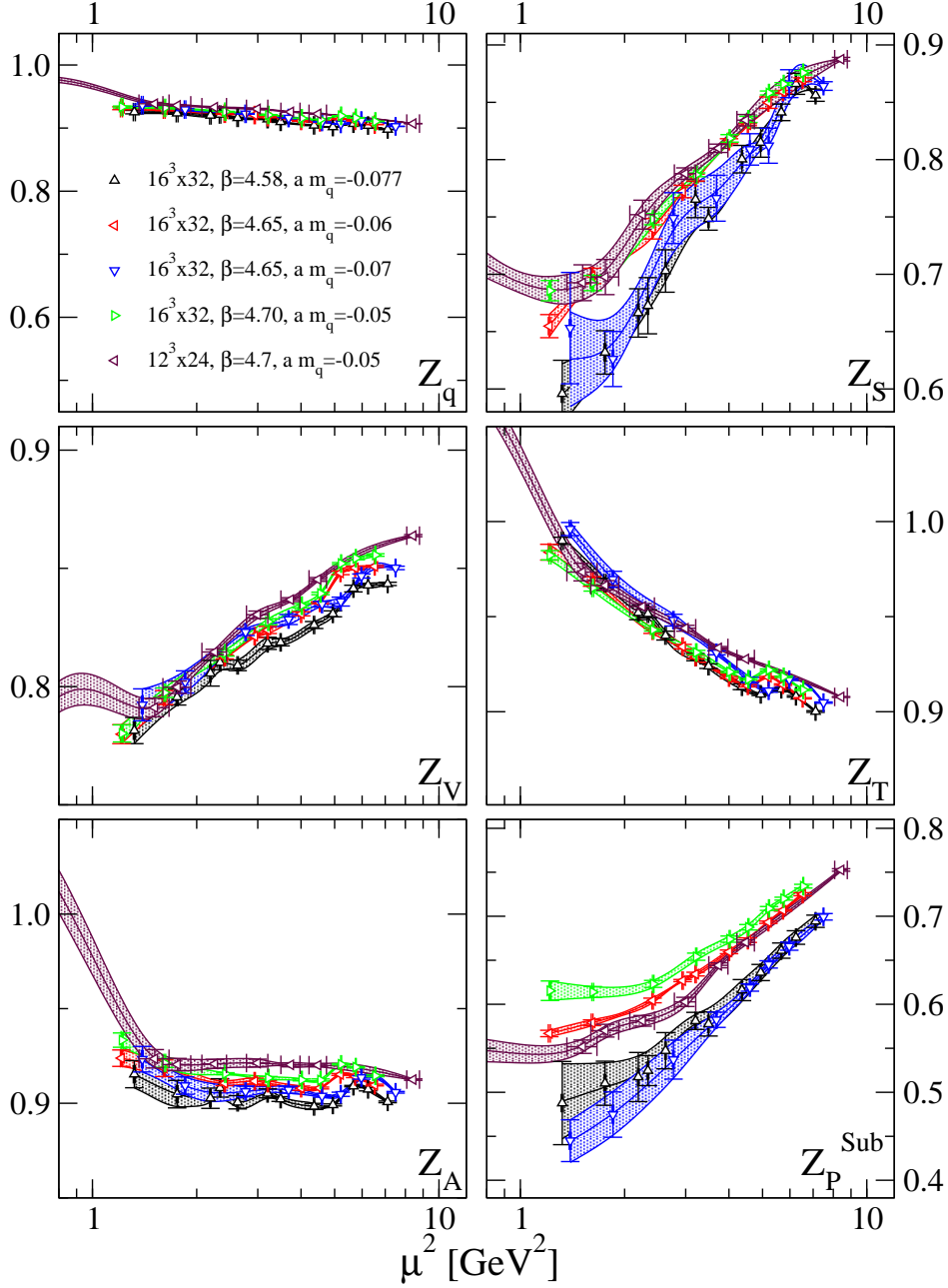


Figure 4: The renormalization factor $Z^{\text{RI}'}$ displayed against μ^2 for $12^3 \times 24$ with $\beta = 4.7$ and all $16^3 \times 32$ lattice setups.

From [45, 46] we get the conversion for the tensors

$$\begin{aligned}
c_T^{\text{RIMS}} = & 1 + \left\{ -\frac{1622}{27} + \frac{184\zeta_3}{9} + \frac{259N_f}{81} \right\} \left(\frac{\alpha_s}{4\pi} \right)^2 + \\
& + \left\{ -\frac{15479317}{5832} + \frac{1209445\zeta_3}{972} + \frac{1072\zeta_4}{81} - \frac{10040\zeta_5}{27} + \right. \\
& + \left(-\frac{1880\zeta_3}{27} + \frac{80\zeta_4}{9} + \frac{225890}{729} \right) N_f + \\
& + \left. \left(-\frac{32\zeta_3}{81} - \frac{9542}{2187} \right) N_f^2 \right\} \left(\frac{\alpha_s}{4\pi} \right)^3 + \mathcal{O} \left(\frac{\alpha_s}{4\pi} \right)^4.
\end{aligned} \tag{4.5}$$

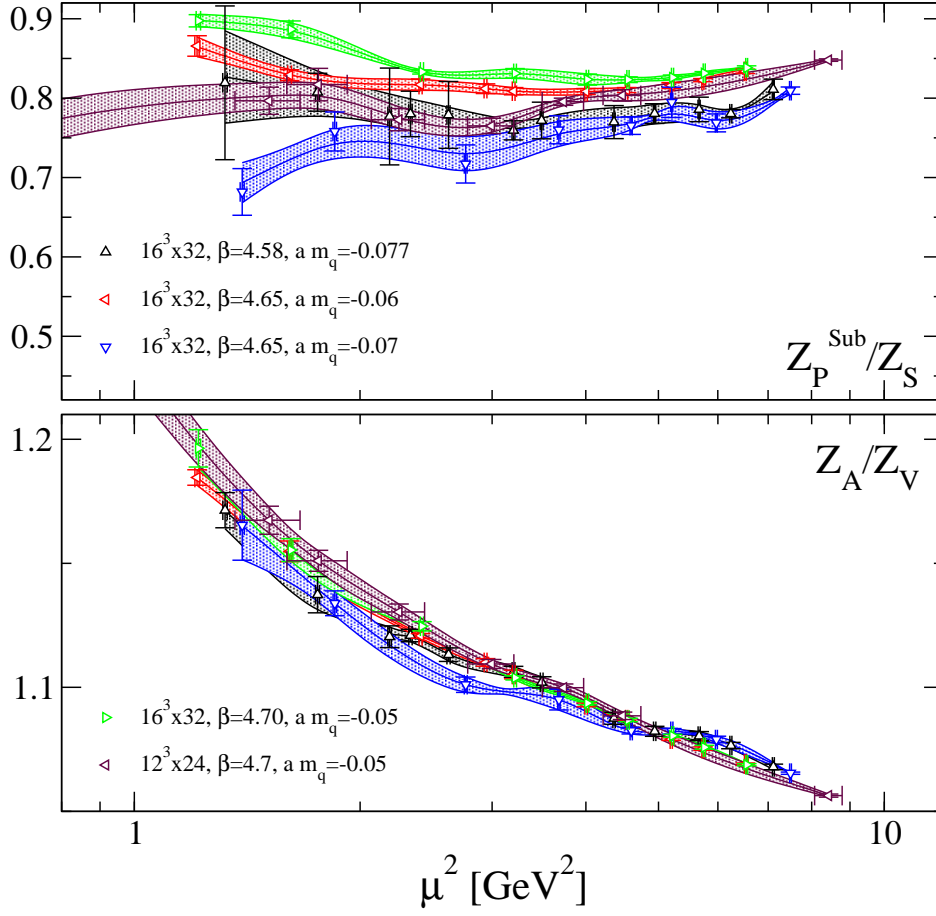


Figure 5: The ratios Z_P^{Sub}/Z_S and Z_A/Z_V vs μ^2 for $12^3 \times 24$ with $\beta = 4.7$ and all $16^3 \times 32$ lattice setups.

Finally for the quark field we use [46]

$$\begin{aligned}
c_q^{\text{R}\overline{\text{MS}}} = & 1 + \left\{ -\frac{1622}{27} + \frac{184\zeta_3}{9} + \frac{259N_f}{81} \right\} \left(\frac{\alpha_s}{4\pi} \right)^2 \\
& + \left\{ -\frac{15479317}{5832} + \frac{1209445\zeta_3}{972} + \frac{1072\zeta_4}{81} - \frac{10040\zeta_5}{27} \right. \\
& + \left(\frac{225890}{729} - \frac{1880\zeta_3}{27} + \frac{80\zeta_4}{9} \right) N_f + \\
& \left. + \left(-\frac{9542}{2187} - \frac{32\zeta_3}{81} \right) N_f^2 \right\} \left(\frac{\alpha_s}{4\pi} \right)^3 + \mathcal{O} \left(\frac{\alpha_s}{4\pi} \right)^4.
\end{aligned} \tag{4.6}$$

The 3-loop expression for the coupling α_s in the $\overline{\text{MS}}$ -scheme [47] reads

$$\begin{aligned}
\frac{\alpha_s(q^2)}{4\pi} = & \frac{1}{\beta_0 \log(q^2)} - \frac{\beta_1}{\beta_0^3} \frac{\log(\log(q^2))}{\log(q^2)^2} \\
& + \frac{1}{\beta_0^5 \log(q^2)^3} \left(\beta_1^2 \log(\log(q^2))^2 - \beta_1^2 \log(\log(q^2)) + \beta_2 \beta_0 - \beta_1^2 \right),
\end{aligned} \tag{4.7}$$

with $q = \mu/\Lambda_{\text{QCD}}$. The QCD scale (from [48] with $r_0 = 0.5 \text{ fm}$) in the $\overline{\text{MS}}$ -scheme is given by

$$\Lambda_{\text{QCD}}^{N_f=2} = 0.243(24) \text{ GeV} \quad (4.8)$$

and we use the following coefficients [49, 50]

$$\beta_0 = 11 - \frac{2}{3}N_f, \quad (4.9a)$$

$$\beta_1 = 102 - \frac{38}{3}N_f, \quad (4.9b)$$

$$\beta_2^{\overline{\text{MS}}} = \frac{2857}{2} - \frac{5033}{18}N_f + \frac{325}{54}N_f^2, \quad (4.9c)$$

$$\begin{aligned} \beta_3^{\overline{\text{MS}}} = & \frac{149753}{6} + 3564\zeta_3 + \left(-\frac{1078361}{162} - \frac{6508\zeta_3}{27} \right) N_f \\ & + \left(-\frac{50065}{162} + \frac{6472\zeta_3}{81} \right) N_f^2 + \frac{1093}{729}N_f^3. \end{aligned} \quad (4.9d)$$

The resulting renormalization factors in the $\overline{\text{MS}}$ -scheme at $\mu = 2 \text{ GeV}$ are collected in Table 5 and Table 6 for the original and the reduced definition, respectively.

4.3 Results in the RGI-form

Renormalization factors in general depend on the renormalization scale μ in a way that is determined by the anomalous dimension γ_O of the operator in consideration

$$\gamma_O(\alpha_s) = -\mu \frac{d}{d\mu} \ln Z_O(\mu^2) = \sum_{i=0}^{\infty} \gamma_i \left(\frac{\alpha_s(\mu^2)}{4\pi} \right)^{i+1}. \quad (4.10)$$

After integrating Eq. (4.10) we arrive at

$$Z^{\text{RGI}} = Z(\mu^2) \left(2\beta_0 \frac{\alpha_s(\mu^2)}{4\pi} \right)^{-\gamma_0/(2\beta_0)} \exp \left\{ \frac{1}{2} \int_0^{\alpha_s(\mu^2)} d\alpha \left(\frac{\gamma(\alpha)}{\beta(\alpha)} + \frac{\gamma_0}{\beta_0\alpha} \right) \right\}, \quad (4.11)$$

the renormalization factor in RGI-form (Renormalization Group Invariant), where the scale dependence coming from the renormalization group is extracted up to a certain order in perturbation theory. We use the the 4-loop expression of the QCD- β -function

$$\beta = \frac{\mu}{2} \frac{d}{d\mu} \alpha_s(\mu^2) = -4\pi \sum_i \beta_i \left(\frac{\alpha}{4\pi} \right)^{i+2}, \quad (4.12)$$

with coefficients listed in Eq. (4.9). Axial vector and vector are scale independent hence their anomalous dimensions are $\gamma_A = \gamma_V = 0$ and therefore $Z_{A,V}^{\text{RGI}} = Z_{A,V}^{\overline{\text{MS}}}$. For γ_q , $\gamma_S = \gamma_P = \gamma_m^{-1}$ and γ_T we use the 4-loop expressions from [49, 51, 45].

In Fig. 6 and Fig. 7 the renormalization factors in RGI-form are displayed against the momentum transfer μ^2 for the $12^3 \times 24$ and $16^3 \times 32$ lattices, respectively. In Fig. 8 the reduced renormalization factors in RGI-form are presented against the same quantity. In the interval $1.5 \text{ GeV} < \mu < 3.0 \text{ GeV}$ we find a maximal deviation from the plateau behavior of 8% for Z_S and 5% for the remaining renormalization factors. In the case of the reduced

factors \overline{Z}_q , \overline{Z}_V , \overline{Z}_A and \overline{Z}_T we observe an almost linear scaling behavior in the region $\mu > 1.55 \text{ GeV}$ or $a\mu > 1.15$. A linear fit of the form $c(1 + d(a\mu)^2)$ allows us to estimate discretization errors proportional to $(a\mu)^2$. For the afore mentioned quantities we find slope values d of 0.019, 0.042, 0.020 and 0.039.

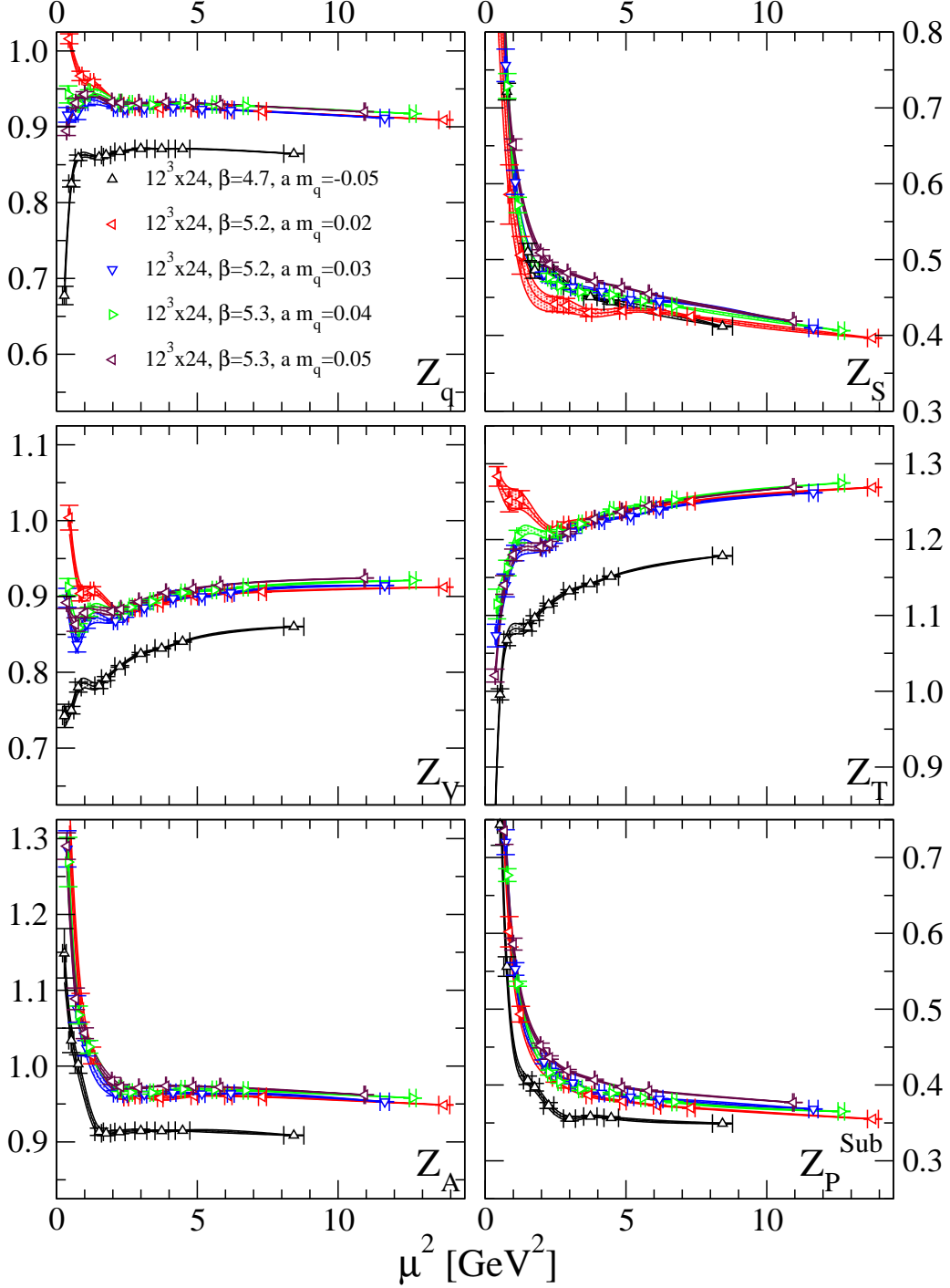


Figure 6: The renormalization factors in RGI-form Z^{RGI} plotted against μ^2 for the $12^3 \times 24$ lattices, runs $a - e$ in Table 1.

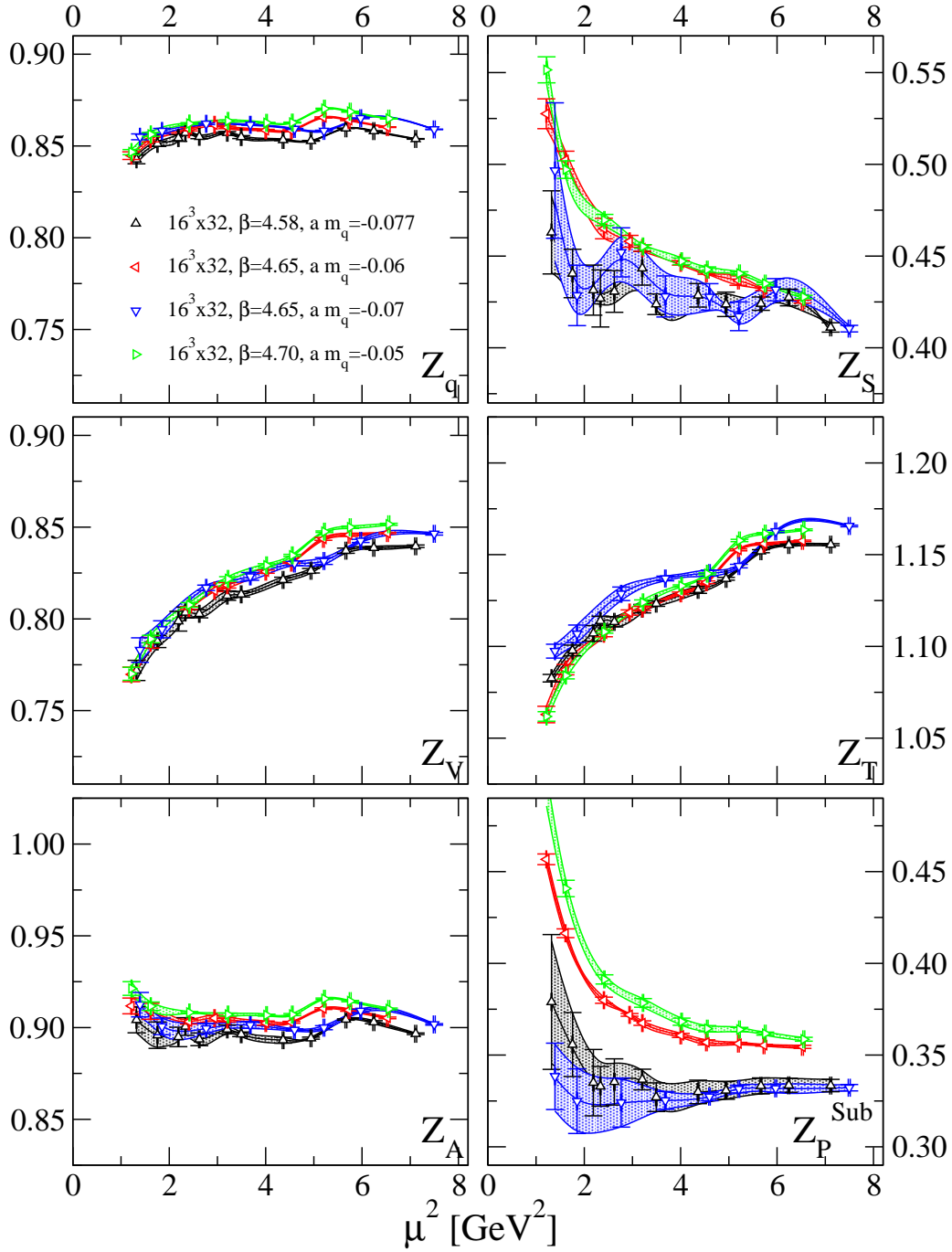


Figure 7: The renormalization factors in RGI-form Z^{RGI} plotted against μ^2 for the $16^3 \times 32$ lattices, runs $f - i$ in Table 1.

4.4 Collection of Results

In this section we collect results of renormalization factors for the original and the reduced method as well as for massive quarks and a chiral extrapolation in Tables 5-8. The same quantities are plotted in Fig. 9 against the lattice spacing. The difference between the

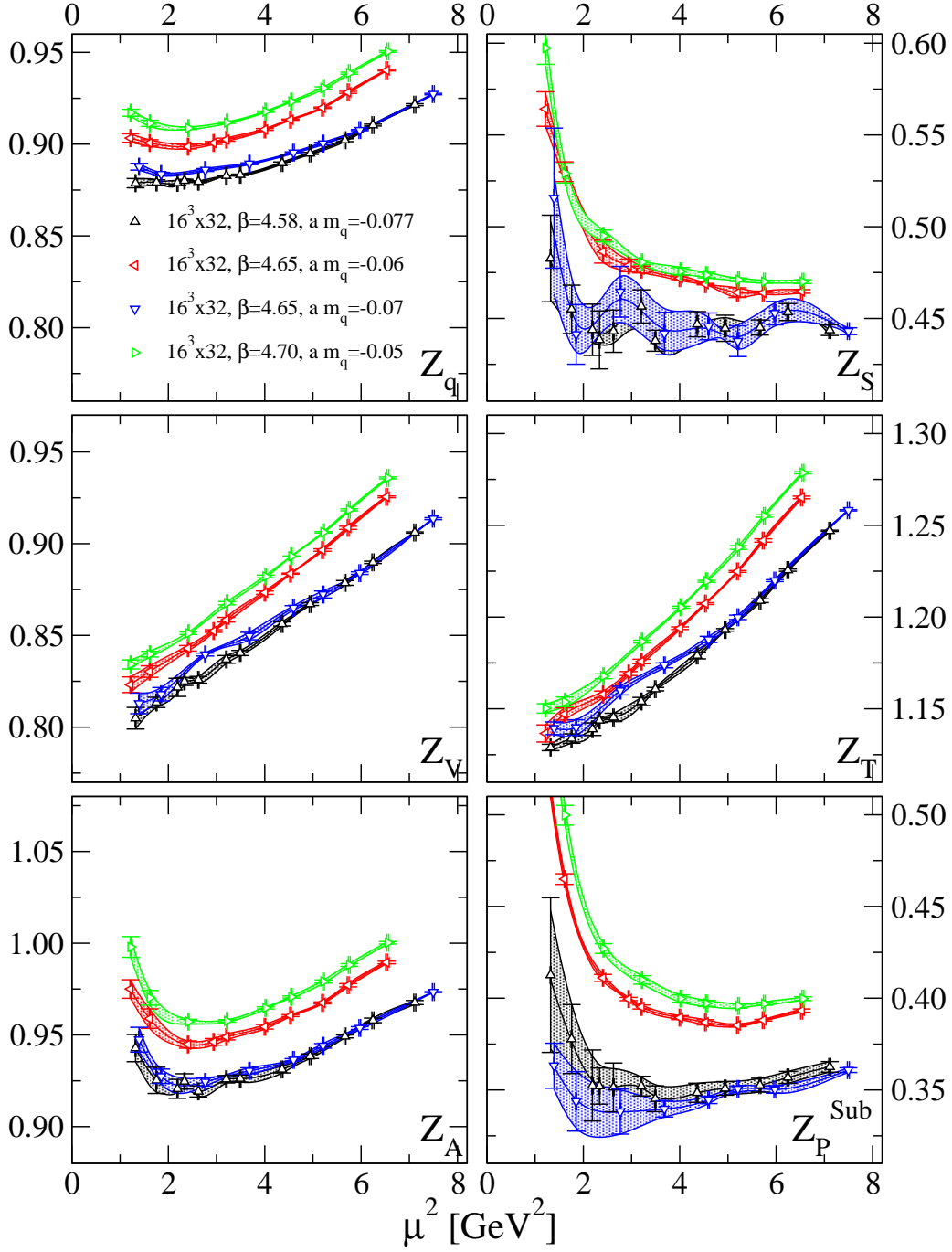


Figure 8: The reduced renormalization factors in RGI-form $\overline{Z}^{\text{RGI}}$ plotted against μ^2 for the $16^3 \times 32$ lattices, runs $f - i$ in Table 1.

original and the reduced method lies in the subtraction of the component of the quark propagator that is proportional to the unit matrix for the latter method (cf. Eq. (2.16)). Thereby a potential cut-off artefact is reduced according to [33]. It is interesting to note that the renormalization factors scalar, vector, tensor and axial vector in the reduced definition

$m_{\text{AWI}}[\text{MeV}]$	$a[\text{fm}]$	Z_q	Z_S	Z_V	Z_T	Z_A	Z_P^{Sub}
31(4)	0.147(18)	0.9116(3)	0.973(4)	0.8345(8)	0.9094(7)	0.915(1)	0.779(3)
43(2)	0.115(6)	0.9672(8)	0.93(1)	0.893(1)	0.976(1)	0.958(2)	0.833(4)
58(3)	0.125(6)	0.9689(7)	0.997(4)	0.896(1)	0.972(1)	0.965(2)	0.849(2)
61(2)	0.120(4)	0.9739(9)	0.989(5)	0.900(2)	0.978(1)	0.968(1)	0.850(3)
76.5(6)	0.129(1)	0.9763(3)	1.021(2)	0.9060(6)	0.9758(5)	0.9739(4)	0.881(2)
35.0(3)	0.150(1)	0.8987(5)	0.969(3)	0.8257(9)	0.8967(5)	0.902(1)	0.783(2)
43.1(5)	0.150(2)	0.9030(3)	0.972(4)	0.8290(9)	0.8998(4)	0.9068(5)	0.800(4)
15.0(4)	0.144(2)	0.8934(7)	0.93(1)	0.818(2)	0.896(2)	0.894(2)	0.71(1)
12.1(5)	0.140(1)	0.9013(3)	0.93(2)	0.826(2)	0.9042(8)	0.901(1)	0.707(8)

Table 5: The interpolated renormalization factors in the $\overline{\text{MS}}$ -scheme $Z^{\overline{\text{MS}}}$ with the corresponding AWI mass m_{AWI} at momentum transfer $\mu = 2 \text{ GeV}$.

$m_{\text{AWI}}[\text{MeV}]$	$a[\text{fm}]$	Z_q	Z_S	Z_V	Z_T	Z_A	Z_P^{Sub}
31(4)	0.147(18)	0.961(1)	1.025(5)	0.8798(9)	0.959(1)	0.964(2)	0.855(3)
43(2)	0.115(6)	1.005(2)	0.97(1)	0.928(2)	1.014(2)	0.995(3)	0.912(5)
58(3)	0.125(6)	1.027(2)	1.057(4)	0.950(2)	1.030(2)	1.023(2)	0.930(2)
61(2)	0.120(4)	1.031(1)	1.047(5)	0.953(2)	1.035(2)	1.024(2)	0.929(3)
76.5(6)	0.129(1)	1.0477(7)	1.096(2)	0.9722(9)	1.047(1)	1.0452(9)	0.976(2)
35.0(3)	0.150(1)	0.9504(5)	1.025(3)	0.8732(9)	0.9483(6)	0.954(1)	0.846(2)
43.1(5)	0.150(2)	0.9604(4)	1.033(4)	0.8817(7)	0.9570(4)	0.9645(6)	0.869(4)
15.0(4)	0.144(2)	0.9278(6)	0.96(1)	0.849(1)	0.930(1)	0.928(2)	0.75(1)
12.1(5)	0.140(1)	0.9327(4)	0.96(2)	0.855(2)	0.9358(9)	0.932(1)	0.740(7)

Table 6: The reduced, interpolated renormalization factors in the $\overline{\text{MS}}$ -scheme $\overline{Z}^{\overline{\text{MS}}}$ with the corresponding AWI mass m_{AWI} at momentum transfer $\mu = 2 \text{ GeV}$.

differ from the original definition solely by a factor \overline{Z}_q/Z_q before taking the chiral limit, which means that the denominator in Eq. (2.19) is not influenced by the redefinition of the quark propagator. For the pseudoscalar renormalization factor we observe a maximum deviation of 5% from this behavior. For chirally extrapolated values this strict factorization is no longer observed, but still holds approximately, with deviations in the sub percent range for vector, tensor and axial vector, and below 3 % and 5 % for the scalar and pseudoscalar, respectively.

5. Summary and Conclusion

Renormalization factors are essential to relate computations of renormalization scheme dependent quantities like the pion decay constant and quark mass on the lattice with results from continuum calculations or measurements. We present values of the renormalization factors for quark bilinears in the regularization independent scheme and the modified minimal subtraction scheme using conventions of [28, 32] and [33]. For the pseudoscalar factor the pion pole is subtracted and a chiral extrapolation was performed.

$m_{\text{AWI}}[\text{MeV}]$	$a[\text{fm}]$	Z_q	Z_S	Z_V	Z_T	Z_A	Z_P^{Sub}
31(4)	0.147(18)	0.9007(3)	0.948(4)	0.8220(7)	0.8992(7)	0.903(1)	0.748(4)
43(2)	0.115(6)	0.9559(8)	0.921(5)	0.880(1)	0.965(1)	0.943(2)	0.806(4)
58(3)	0.125(6)	0.9519(8)	0.958(3)	0.877(1)	0.957(1)	0.945(2)	0.817(3)
61(2)	0.120(4)	0.957(1)	0.949(2)	0.882(2)	0.964(2)	0.949(1)	0.820(4)
76.5(6)	0.129(1)	0.9532(4)	0.976(1)	0.8814(6)	0.9563(6)	0.9489(5)	0.841(2)
35.0(3)	0.150(1)	0.8860(5)	0.943(2)	0.8112(7)	0.8856(6)	0.8883(7)	0.761(3)
43.1(5)	0.150(2)	0.8880(2)	0.945(1)	0.812(1)	0.8873(4)	0.8910(6)	0.774(5)
15.0(4)	0.144(2)	0.8887(7)	0.918(7)	0.813(2)	0.892(2)	0.889(1)	0.69(2)
12.1(5)	0.140(1)	0.8974(3)	0.920(6)	0.822(2)	0.9015(7)	0.896(1)	0.70(2)

Table 7: A chiral extrapolation for the interpolated renormalization factors in the $\overline{\text{MS}}$ -scheme $Z^{\overline{\text{MS}},\text{chir}}$ with the corresponding AWI mass m_{AWI} at momentum transfer $\mu = 2 \text{ GeV}$.

$m_{\text{AWI}}[\text{MeV}]$	$a[\text{fm}]$	Z_q	Z_S	Z_V	Z_T	Z_A	Z_P^{Sub}
31(4)	0.147(18)	0.925(1)	0.969(5)	0.8453(9)	0.925(1)	0.928(2)	0.799(4)
43(2)	0.115(6)	0.957(1)	0.891(6)	0.878(2)	0.967(2)	0.940(3)	0.849(4)
58(3)	0.125(6)	0.962(1)	0.956(4)	0.884(2)	0.967(2)	0.954(2)	0.868(3)
61(2)	0.120(4)	0.965(1)	0.939(3)	0.886(2)	0.972(2)	0.955(2)	0.867(4)
76.5(6)	0.129(1)	0.9636(6)	0.971(2)	0.8903(8)	0.9672(9)	0.9590(7)	0.896(2)
35.0(3)	0.150(1)	0.9091(5)	0.959(2)	0.8267(7)	0.9087(6)	0.9061(8)	0.806(2)
43.1(5)	0.150(2)	0.9115(3)	0.960(1)	0.8314(8)	0.9107(4)	0.9134(7)	0.819(5)
15.0(4)	0.144(2)	0.9124(6)	0.941(7)	0.834(2)	0.916(1)	0.912(2)	0.72(2)
12.1(5)	0.140(1)	0.9202(4)	0.942(6)	0.842(1)	0.9237(7)	0.919(1)	0.72(2)

Table 8: A chiral extrapolation for the reduced, interpolated renormalization factors in the $\overline{\text{MS}}$ -scheme $Z^{\overline{\text{MS}},\text{chir}}$ with the corresponding AWI mass m_{AWI} at momentum transfer $\mu = 2 \text{ GeV}$.

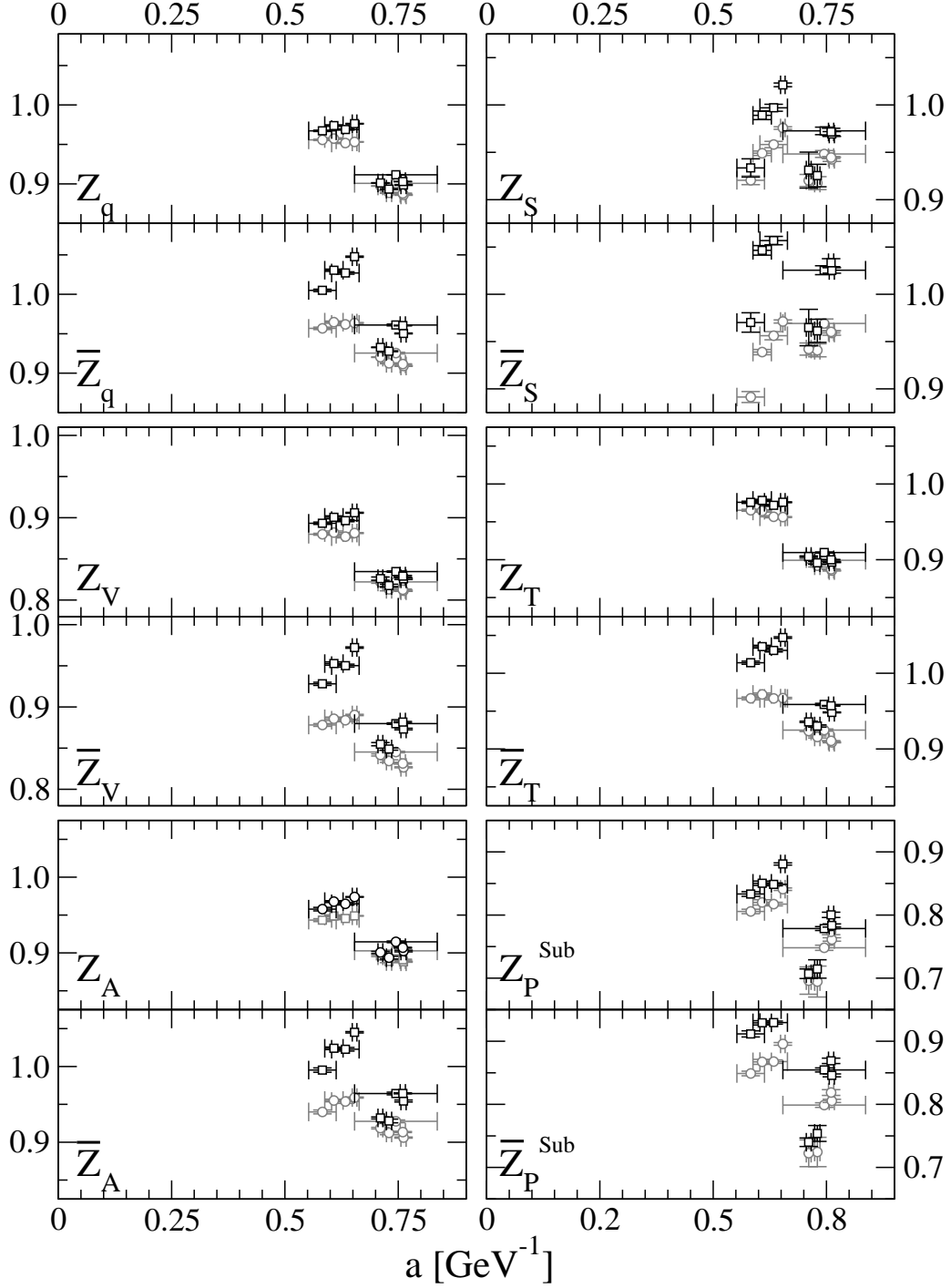


Figure 9: The interpolated renormalization factors in the $\overline{\text{MS}}$ -scheme $Z^{\overline{\text{MS}}}$ and $\overline{Z}^{\overline{\text{MS}}}$ at momentum transfer $\mu = 2 \text{ GeV}$ plotted against the lattice spacing a for massive quarks (black) and a chiral extrapolation (gray).

Acknowledgments

This work is based on gauge configurations obtained from the BGR collaboration on the SGI Altix 4700 of the Leibniz-Rechenzentrum Munich. The quark propagators have been determined on the Sun Fire V20z cluster of the computer center of Karl-Franzens-Universität Graz.

I am deeply grateful for the support Christian Lang gave me and for our many interesting discussions. I also appreciate the help of Meinulf Gökeler very much.

References

- [1] P. H. Ginsparg and K. G. Wilson, *A remnant of chiral symmetry on the lattice*, *Phys. Rev.* **D25** (1982) 2649.
- [2] M. Lüscher, *Exact chiral symmetry on the lattice and the Ginsparg-Wilson relation*, *Phys. Lett.* **B428** (1998) 342–345, [[hep-lat/9802011](#)].
- [3] R. Narayanan and H. Neuberger, *Chiral fermions on the lattice*, *Phys. Rev. Lett.* **71** (1993) 3251–3254, [[hep-lat/9308011](#)].
- [4] R. Narayanan and H. Neuberger, *Infinitely many regulator fields for chiral fermions*, *Phys. Lett.* **B302** (1993) 62–69, [[hep-lat/9212019](#)].
- [5] P. Hasenfratz and F. Niedermayer, *Perfect lattice action for asymptotically free theories*, *Nucl. Phys.* **B414** (1994) 785–814, [[hep-lat/9308004](#)].
- [6] C. Gattringer, *A new approach to Ginsparg-Wilson fermions*, *Phys. Rev.* **D63** (2001) 114501, [[hep-lat/0003005](#)].
- [7] D. B. Kaplan, *A Method for simulating chiral fermions on the lattice*, *Phys. Lett.* **B288** (1992) 342–347, [[hep-lat/9206013](#)].
- [8] V. Furman and Y. Shamir, *Axial symmetries in lattice QCD with Kaplan fermions*, *Nucl. Phys.* **B439** (1995) 54–78, [[hep-lat/9405004](#)].
- [9] **BGR** Collaboration, C. Gattringer *et al.*, *Quenched spectroscopy with fixed-point and chirally improved fermions*, *Nucl. Phys.* **B677** (2004) 3–51, [[hep-lat/0307013](#)].
- [10] C. B. Lang, P. Majumdar, and W. Ortner, *QCD with two dynamical flavors of chirally improved quarks*, *Phys. Rev.* **D73** (2006) 034507, [[hep-lat/0512014](#)].
- [11] C. B. Lang, P. Majumdar, and W. Ortner, *First results from dynamical chirally improved fermions*, *PoS LAT2005* (2006) 131, [[hep-lat/0509005](#)].
- [12] C. Gattringer *et al.*, *Hadron Spectroscopy with Dynamical Chirally Improved Fermions*, *Phys. Rev.* **D79** (2009) 054501, [[arXiv:0812.1681](#)].
- [13] C. Gattringer, I. Hip, and C. B. Lang, *Approximate Ginsparg-Wilson fermions: A first test*, *Nucl. Phys.* **B597** (2001) 451–474, [[hep-lat/0007042](#)].
- [14] C. Gattringer, M. Gökeler, P. Huber, and C. B. Lang, *Renormalization of bilinear quark operators for the chirally improved lattice dirac operator*, *Nucl. Phys.* **B694** (2004) 170–186, [[hep-lat/0404006](#)].
- [15] V. Gimenez, L. Giusti, F. Rapuano, and M. Talevi, *Non-perturbative renormalization of quark bilinears*, *Nucl. Phys.* **B531** (1998) 429–445, [[hep-lat/9806006](#)].

- [16] A. Donini, V. Gimenez, G. Martinelli, M. Talevi, and A. Vladikas, *Non-perturbative renormalization of lattice four-fermion operators without power subtractions*, *Eur. Phys. J.* **C10** (1999) 121–142, [[hep-lat/9902030](#)].
- [17] L. Giusti, V. Gimenez, F. Rapuano, M. Talevi, and A. Vladikas, *Quark masses and the chiral condensate with a non-perturbative renormalization procedure*, *Nucl. Phys. Proc. Suppl.* **73** (1999) 210–212, [[hep-lat/9809037](#)].
- [18] D. Becirevic *et al.*, *Non-perturbatively Renormalized Light-Quark Masses with the Alpha Action*, *Phys. Lett.* **B444** (1998) 401–410, [[hep-lat/9807046](#)].
- [19] **JLQCD** Collaboration, N. Ishizuka *et al.*, *Non-perturbative renormalization factors of bilinear quark operators for Kogut-Susskind fermions and light quark masses in quenched QCD*, *Nucl. Phys. Proc. Suppl.* **73** (1999) 279–281, [[hep-lat/9809124](#)].
- [20] T. Blum *et al.*, *Non-perturbative renormalisation of domain wall fermions: Quark bilinears*, *Phys. Rev.* **D66** (2002) 014504, [[hep-lat/0102005](#)].
- [21] L. Giusti, C. Hölbling, and C. Rebbi, *Light quark masses with overlap fermions in quenched QCD*, *Phys. Rev.* **D64** (2001) 114508, [[hep-lat/0108007](#)].
- [22] J. B. Zhang *et al.*, *Nonperturbative renormalization of composite operators with overlap fermions*, *Phys. Rev.* **D72** (2005) 114509, [[hep-lat/0507022](#)].
- [23] T. A. DeGrand and Z.-f. Liu, *Renormalization of bilinear quark operators for overlap fermions*, *Phys. Rev.* **D72** (2005) 054508, [[hep-lat/0507017](#)].
- [24] J. Noaki *et al.*, *Non-perturbative renormalization of bilinear operators with dynamical overlap fermions*, [arXiv:0907.2751](#).
- [25] A. Skouroupathis and H. Panagopoulos, *Two-loop renormalization of vector, axial-vector and tensor fermion bilinears on the lattice*, *Phys. Rev.* **D79** (2009) 094508, [[arXiv:0811.4264](#)].
- [26] A. Skouroupathis and H. Panagopoulos, *Two-loop renormalization of fermion bilinear operators on the lattice*, [arXiv:1002.3513](#).
- [27] M. Gockeler *et al.*, *Perturbative and Nonperturbative Renormalization in Lattice QCD*, [arXiv:1003.5756](#).
- [28] G. Martinelli, C. Pittori, C. T. Sachrajda, M. Testa, and A. Vladikas, *A general method for nonperturbative renormalization of lattice operators*, *Nucl. Phys.* **B445** (1995) 81–108, [[hep-lat/9411010](#)].
- [29] M. L. Paciello, S. Petrarca, B. Taglienti, and A. Vladikas, *Gribov noise of the lattice axial current renormalization constant*, *Phys. Lett.* **B341** (1994) 187–194, [[hep-lat/9409012](#)].
- [30] L. Giusti, M. L. Paciello, C. Parrinello, S. Petrarca, and B. Taglienti, *Problems on lattice gauge fixing*, *Int. J. Mod. Phys.* **A16** (2001) 3487–3534, [[hep-lat/0104012](#)].
- [31] L. Giusti, S. Petrarca, B. Taglienti, and N. Tantalo, *Remarks on the gauge dependence of the RI/MOM renormalization procedure*, *Phys. Lett.* **B541** (2002) 350–355, [[hep-lat/0205009](#)].
- [32] M. Gockeler *et al.*, *Nonperturbative renormalisation of composite operators in lattice QCD*, *Nucl. Phys.* **B544** (1999) 699–733, [[hep-lat/9807044](#)].
- [33] S. Capitani *et al.*, *Renormalisation and off-shell improvement in lattice perturbation theory*, *Nucl. Phys.* **B593** (2001) 183–228, [[hep-lat/0007004](#)].

- [34] V. Maillart and F. Niedermayer, *A specific lattice artefact in non-perturbative renormalization of operators*, [arXiv:0807.0030](#).
- [35] M. Lüscher and P. Weisz, *Computation of the action for on-shell improved lattice gauge theories at weak coupling*, *Phys. Lett.* **B158** (1985) 250.
- [36] C. Morningstar and M. J. Peardon, *Analytic smearing of $SU(3)$ link variables in lattice QCD*, *Phys. Rev.* **D69** (2004) 054501, [[hep-lat/0311018](#)].
- [37] J.-R. Cudell, A. Le Yaouanc, and C. Pittori, *Pseudoscalar vertex, Goldstone boson and quark masses on the lattice*, *Phys. Lett.* **B454** (1999) 105–114, [[hep-lat/9810058](#)].
- [38] J. R. Cudell, A. Le Yaouanc, and C. Pittori, *Large pion pole in $Z(S)(MOM)/(Z(P)(MOM)$ from Wilson action data*, *Phys. Lett.* **B516** (2001) 92–102, [[hep-lat/0101009](#)].
- [39] L. Giusti and A. Vladikas, *RI/MOM renormalization window and Goldstone pole contamination*, *Phys. Lett.* **B488** (2000) 303–312, [[hep-lat/0005026](#)].
- [40] D. Becirevic *et al.*, *Renormalization constants of quark operators for the non-perturbatively improved Wilson action*, *JHEP* **08** (2004) 022, [[hep-lat/0401033](#)].
- [41] Y. Aoki *et al.*, *Non-perturbative renormalization of quark bilinear operators and B_K using domain wall fermions*, *Phys. Rev.* **D78** (2008) 054510, [[arXiv:0712.1061](#)].
- [42] M. F. L. Golterman and K.-C. Leung, *Applications of Partially Quenched Chiral Perturbation Theory*, *Phys. Rev.* **D57** (1998) 5703–5710, [[hep-lat/9711033](#)].
- [43] E. Franco and V. Lubicz, *Quark mass renormalization in the \overline{MS} -bar and RI schemes up to the NNLO order*, *Nucl. Phys.* **B531** (1998) 641–651, [[hep-ph/9803491](#)].
- [44] K. G. Chetyrkin and A. Retey, *Renormalization and running of quark mass and field in the regularization invariant and \overline{MS} -bar schemes at three and four loops*, *Nucl. Phys.* **B583** (2000) 3–34, [[hep-ph/9910332](#)].
- [45] J. A. Gracey, *Three loop \overline{MS} -bar tensor current anomalous dimension in QCD*, *Phys. Lett.* **B488** (2000) 175–181, [[hep-ph/0007171](#)].
- [46] J. A. Gracey, *Three loop anomalous dimension of non-singlet quark currents in the RI' scheme*, *Nucl. Phys.* **B662** (2003) 247–278, [[hep-ph/0304113](#)].
- [47] A. I. Alekseev, *Strong coupling constant to four loops in the analytic approach to QCD*, *Few Body Syst.* **32** (2003) 193–217, [[hep-ph/0211339](#)].
- [48] M. Göckeler *et al.*, *A determination of the lambda parameter from full lattice QCD*, *Phys. Rev.* **D73** (2006) 014513, [[hep-ph/0502212](#)].
- [49] T. van Ritbergen, J. A. M. Vermaseren, and S. A. Larin, *The four-loop beta function in quantum chromodynamics*, *Phys. Lett.* **B400** (1997) 379–384, [[hep-ph/9701390](#)].
- [50] M. Czakon, *The four-loop QCD beta-function and anomalous dimensions*, *Nucl. Phys.* **B710** (2005) 485–498, [[hep-ph/0411261](#)].
- [51] K. G. Chetyrkin, *Quark mass anomalous dimension to $o(\alpha(s)^{**4})$* , *Phys. Lett.* **B404** (1997) 161–165, [[hep-ph/9703278](#)].